



# CHORUS

This is the accepted manuscript made available via CHORUS. The article has been published as:

## Determination of Viral Capsid Elastic Properties from Equilibrium Thermal Fluctuations

Eric R. May and Charles L. Brooks, III

Phys. Rev. Lett. **106**, 188101 — Published 2 May 2011

DOI: [10.1103/PhysRevLett.106.188101](https://doi.org/10.1103/PhysRevLett.106.188101)

# Determination of Viral Capsid Elastic Properties from Equilibrium Thermal Fluctuations

Eric R. May and Charles L. Brooks III\*

*Department of Chemistry and Biophysics Program, University of Michigan, Ann Arbor, MI 48109\**

We apply two-dimensional elasticity theory to viral capsids to develop a framework for calculating elastic properties of viruses from equilibrium thermal fluctuations of the capsid surface in molecular dynamics and elastic network model trajectories. We show that the magnitudes of the long wave length modes of motion available in a simulation with all atomic degrees of freedom are recapitulated by an elastic network model. For the mode spectra to match, the elastic network model must be scaled appropriately by a factor which can be determined from an icosahedrally constrained all-atom simulation. With this method we calculate the two-dimensional Young's modulus,  $Y$ , bending modulus,  $\kappa$ , and Foppl-von Kármán number,  $\gamma$ , for the  $T=1$  mutant of the Sesbania mosaic virus. The values determined are in the range of previous theoretical estimates.

The material properties of capsids is of interest for nanotechnology design purposes, but also for understanding the morphology of spherical viruses. When examining the structures of spherical viruses, a range of sizes and sphericities are observed [1]. The continuum elastic theory of buckling transitions has been applied to predict the equilibrium configurations of spherical [2] and non spherical capsids [3]. In the case of spherical capsids, the theory predicts a transition from spherical to faceted icosahedral geometries as a function of the dimensionless Foppl-von Kármán number,  $\gamma = YR^2/\kappa$ , where  $Y$  is the two dimensional Young's modulus,  $\kappa$  is the bending modulus and  $R$  is the shell radius. The buckling transition has been proposed as a maturation mechanism for the bacteriophage HK97 ( $T=7$ ) during which the capsid swells and changes from a spherical to a faceted icosahedral shape [4].

Experimental studies have also been directed toward the assessment of mechanical properties of capsids, primarily using the technique of atomic force microscopy (AFM). The first AFM studies involving viruses measured the forces related to packing and unpacking of DNA into bacteriophage capsids and the internal pressure inside a capsid [5–7]. More recent studies, using AFM, have performed nanoindentation on both empty and RNA filled capsids to probe the stress-strain behavior and measured a linear spring constant [8–10]. These studies have increased our understanding of the material properties of capsids and provided estimates of the three dimensional Young's modulus,  $E$ , but have not determined the two-dimensional parameters.

In the present work, we begin by deriving a relationship between measurable surface properties (spherical harmonic expansion coefficients) and the elastic properties of interest ( $Y$  and  $\kappa$ ). The forces acting on a spherical shell due to in-plane and radial deformations have been described previously [11]. We take as our starting point a simplification of these force equations by considering only radial deformations, shown in Eq. (1) and Eq. (2)

$$F^\alpha = (\lambda + \mu)D^\alpha \left( \frac{2\zeta}{R} \right) \quad (1)$$

$$N = -(\lambda + \mu) \left( \frac{4\zeta}{R^2} \right) - \kappa \mathcal{L}\zeta. \quad (2)$$

where  $F^\alpha$  and  $N$  are the lateral and normal forces, respectively,  $\lambda$  and  $\mu$  are the Lamé constants,  $\zeta$  is a normal deformation,  $\mathcal{L}$  is the operator given by  $\mathcal{L} = D_\alpha D^\alpha D_\beta D^\beta + \frac{2}{R^2} D_\alpha D^\alpha$ ,  $D_\alpha$  and  $D^\alpha$  are covariant and contravariant differential operators, respectively, and the indices  $\alpha$  and  $\beta$  take on values of 1 or 2 to indicate the lateral direction on the surface. When we calculate the deformations of the viral capsid surface during our simulations, we do so by considering only the normal displacements ( $\zeta$ ) on a fixed grid (in the polar and azimuthal directions). In this framework, the three-dimensional motions of atoms are projected onto the one-dimensional radial displacement of an element. By considering only radial displacements we are making an approximation to the full 3D forces equations, which simplifies the mathematical manipulations. Furthermore, we believe that the center of mass displacements of surface elements will be dominated by the radial displacements (we validate this assertion later in the paper). When we compute the displacement function,  $\zeta(\theta, \phi, t)$ , at a given moment in time, we do so by considering the difference between the instantaneous surface,  $r(\theta, \phi, t)$ , and the ensemble averaged surface,  $\langle r(\theta, \phi) \rangle$ .  $\zeta$  can be decomposed using a spherical harmonic basis set

$$\zeta(\theta, \phi, t) \equiv r(\theta, \phi, t) - \langle r(\theta, \phi) \rangle = \sum_{l=0}^{l_{max}} \sum_{m=-l}^{+l} a_{lm} Y_{lm}(\theta, \phi). \quad (3)$$

$Y_{lm}$  are spherical harmonics, which are eigenfunctions of the operators in Eq. (1) - (2), allowing for the forces to be written in terms of the eigenvalues [11],

$$\begin{bmatrix} F^1 \\ F^2 \\ N \end{bmatrix} = -\mathbf{\Lambda}\mathbf{d}, \quad (4)$$

$$\begin{aligned} \text{where } \Lambda_{11} = \Lambda_{22} &= \frac{2(\lambda + \mu)}{R^2}, \\ \Lambda_{33} &= \frac{4(\lambda + \mu)}{R^2} + \kappa \frac{l(l-1)(l+1)(l+2)}{R^4}, \quad \Lambda_{i \neq j} = 0 \\ \text{and } d_{i=1,2,3} &= \zeta. \end{aligned}$$

The elastic energy density is given by  $\tilde{E} = \frac{1}{2}\mathbf{d} \cdot \mathbf{\Lambda}\mathbf{d}$ . The total elastic energy,  $E$ , of the surface can then be obtained by integration over the surface

$$E = \frac{1}{2} \int_{\phi} \int_{\theta} \sum_l \left( \frac{8b}{R^2} + \kappa \frac{l(l-1)(l+1)(l+2)}{R^4} \right) \times \sum_{m=-l}^{+l} a_{lm} Y_{lm} \left[ \sum_{l'} \sum_{m'=-l'}^{+l'} a_{l'm'}^* Y_{l'm'}^* \right] R^2 d\Omega \quad (5)$$

where  $b \equiv \lambda + \mu$ ,  $\Omega$  is the solid angle and  $*$  indicates the complex conjugate. The orthogonality of the spherical harmonics and the definition,  $|\hat{a}_l|^2 \equiv \sum_{m=-l}^{+l} a_{lm} a_{lm}^*$ , allow the total elastic energy to be written in simplified form

$$E = \frac{1}{2} \sum_l \left( 8b + \kappa \frac{l(l-1)(l+1)(l+2)}{R^2} \right) |\hat{a}_l|^2. \quad (6)$$

Given the quadratic form of the energy, the ensemble averages of  $|\hat{a}_l|^2$  can be calculated and a relationship is obtained which contains only measurable surface properties ( $R$ ,  $\langle |\hat{a}_l|^2 \rangle$ ) and elastic parameters ( $\lambda$ ,  $\mu$ ,  $\kappa$ )

$$\langle |\hat{a}_l|^2 \rangle = \frac{k_B T}{8b + \kappa \frac{l(l-1)(l+1)(l+2)}{R^2}}. \quad (7)$$

From fitting the spectral intensities to Eq. 7,  $\kappa$  and  $b$  can be determined. The elastic parameter relationships (see supplementary material), allow for  $Y$  to be determined when a value for the Poisson ratio,  $\sigma$ , is assumed (we choose  $\sigma = 0.3$  [12])

The theory described here is based upon deformations of spherical shells, and while we will be applying this method to spherical capsids, in actuality the capsids deviate from pure sphericity. The deformations we compute are radial, but not necessarily normal to the capsid surface. Defining the surface normal is not a straightforward calculation and therefore we are introducing an approximation into our calculation, however we believe this error arising from this approximation will be small. The more spherical the virus, the smaller the error, and therefore we calculate the capsid asphericity ( $A$ ) as a gauge for

understanding potential errors,  $A = \frac{1}{N} \sum_{i=1}^N \frac{(R_i - \langle R \rangle)^2}{\langle R \rangle^2}$ , where  $N$  is the number of surface grid points and  $R_i$  is the radius at each grid point.

The system we study in this work is the Sesbania mosaic virus (SeMV), an RNA plant virus. The wild-type SeMV forms a  $T=3$  capsid, but deletion of the 31 N-terminal residues results in formation of a mutant  $T=1$  particle [13], shown in Fig. 1A. The asphericity of this structure is  $10^{-3}$ , which is an intermediate degree of faceting [2]. In this work, we focus exclusively on the  $T=1$  capsid, as the reduced size allows us to access longer simulation times. Furthermore, it has been unclear at what size of capsid it is appropriate to apply continuum elasticity theory. We provide evidence that even the smallest class of virus ( $T=1$ ) can be suitably treated in this manner, as we observe surface thermal fluctuations of the capsid to be well described by the elastic model in Eq. 7.

To generate the surface fluctuations we carried out a molecular dynamics (MD) simulation of the complete  $T=1$  SeMV capsid, including explicit water and ions. After the system equilibrates, spherical harmonic decomposition of  $\zeta$ , according to Eq. (3) with  $l_{max}=11$ , is performed every 1 ps. Further details regarding the simulation protocol and surface fluctuation decomposition are presented in the supplementary material.

The coefficients,  $\langle |\hat{a}_l|^2 \rangle$ , are calculated and plotted against the mode number,  $l$ , in Fig. 1B(●). Modes with  $l < 2$  correspond to uniform expansion ( $l = 0$ ) and polar and equatorial dimpling ( $l = 1$ ); the surface deformations minimally project onto these modes and the fitting is performed on modes with  $l \geq 2$ . The highest mode we fit is for  $l=6$ , as higher modes deviate from the theoretical model given by Eq. (7). We attribute this behavior to a breakdown in the continuum model at short wavelengths, where the molecular behavior becomes more dominant. The length scale at which the breakdown occurs coincides with the dimension of the subunit (also roughly the thickness of the shell). A rough estimate of the subunit diameter (assuming a spherical shell and spherical subunit) is 4 nm; the corresponding Nyquist critical frequency is therefore  $0.125 \text{ nm}^{-1}$ . The frequency of  $Y_{l=6,m=0}$  is  $0.122 \text{ nm}^{-1}$  and  $Y_{l=7,m=0}$  is  $0.142 \text{ nm}^{-1}$ , therefore the breakdown should occur between  $l = 6$  and  $l = 7$ , which is what is observed. This change in regime for thermal fluctuations at higher frequency has also been observed in several simulations of lipid bilayers at lengths below the bilayer thickness [14, 15].

From the fit to the lower frequency modes in Fig. 1B(●), we determine  $Y = 35.4 k_B T / \text{nm}^2$ ,  $\kappa = 39.7 k_B T$ , and  $\gamma = 54.1$ . Our calculation of the ratio of elastic parameters,  $Y/\kappa \approx \text{nm}^{-2}$ , is consistent with a previous theoretical study in which continuum elastic shells were fit to experimentally determined capsid structures [2], the absolute magnitudes are also in the range of previous predictions. Theoretical estimates, and estimates based on

AFM experiments, have predicted  $Y$  to be in the range of 10 - 250  $k_B T/\text{nm}^2$  and  $\kappa$  to be in the range of 10 - 250  $k_B T$  [3, 8, 16, 17]. For an additional consistency check we compute an effective mechanical thickness from the values of  $Y$  and  $\kappa$  and compare this value to our measured value of 1.9 nm. The mechanical thickness,  $h$ , can be estimated from the equations which relate the 2D quantities to the 3D Young's modulus,  $E$  (see supplementary material) [18]. The effective mechanical thickness we calculate is 2.6 nm, which agrees with the measured value of 1.9 nm, and supports our estimates of  $Y$  and  $\kappa$ .

Conducting all-atom MD simulations of small virus capsids is becoming more attainable with increasing computing power [19], however, examining larger structures ( e.g.  $T \geq 7$ ) will require utilization of less expensive calculation methodologies. Elastic network models (ENM) and normal mode analysis (NMA) have been used extensively in studying protein dynamics [20], including viruses [12, 21] and we have explored using ENMs for computing virus dynamics. An ENM for the SeMV  $T = 1$  structure was constructed and the normal modes were calculated using the rotation-translation block method [22, 23]. The network is propagated according to  $\Delta \mathbf{r}_n(t) = \sum_{i=7}^N C_i \boldsymbol{\alpha}_n^i \cos(\omega_i t + \psi_i)$  where,  $\Delta \mathbf{r}_n$  is the displacement vector of atom  $n$ ,  $\boldsymbol{\alpha}_n^i$  is the Eigenvector of mode  $i$  projected onto atom  $n$ ,  $\omega$  is the frequency of the mode,  $\psi$  is a random phase shift of the mode and  $C$  is the amplitude of the mode. We choose to set the amplitude the same for all modes and choose a value for  $C$  that produces a root mean square atomic fluctuations of 1 Å, which are typical of the thermal scale (300 K). Further details about the ENM construction and propagation and the NMA of the network is presented in the supplementary material. The resultant spherical harmonic mode magnitudes  $\langle |\hat{a}_l|^2 \rangle_{ENM}$  can then be rescaled such that the sum of the modes from the ENM matches the sum of modes from an MD simulation

$$\langle |\hat{a}_l|^2 \rangle = \frac{(\sum_l \langle |\hat{a}_l|^2 \rangle_{MD})}{(\sum_l \langle |\hat{a}_l|^2 \rangle_{ENM})} \langle |\hat{a}_l|^2 \rangle_{ENM} . \quad (8)$$

This rescaling indicates an MD trajectory must also be preformed, however, we can exploit the icosahedral symmetry of the virus to calculate  $\sum_l \langle |\hat{a}_l|^2 \rangle_{MD}$  by conducting a MD simulation of only the asymmetric unit of the virus under icosahedral boundary conditions [24]. From Eq. 7 we should expect that two simulations of the same system at the same temperature to produce the same  $\sum_l \langle |\hat{a}_l|^2 \rangle$ . The enforcement of icosahedral symmetry will redistribute the modes magnitudes, however, the sum of the modes should be conserved. We compare the spectrum of both the unconstrained ( $\bullet$ ) and icosahedrally constrained ( $\blacktriangle$ ) MD simulations in Fig. 1B and close agreement of sums of the modes are observed:  $\sum_l \langle |\hat{a}_l|^2 \rangle_{\text{Complete Capsid}} = 1.78 \times 10^{-2} \text{ nm}^2$ ,

$\sum_l \langle |\hat{a}_l|^2 \rangle_{\text{Icosahedrally Constrained}} = 1.62 \times 10^{-2} \text{ nm}^2$ . Most of the motion of the icosahedral system is accounted for by modes  $l = 0, 6, 10$ , and naturally, these are the spherical harmonics which are also icosahedrally symmetric [2]. Further details on the asymmetric unit simulation under icosahedral boundary conditions are presented in the supplementary material.

We fit the renormalized ENM spectral intensity in the long wave length range ( $l \leq 6$ ) and compare it to the unconstrained MD spectrum in Fig. 1C. There is strong agreement between the two models. From the ENM spectral intensities we calculated  $Y = 31.7 k_B T/\text{nm}^2$ ,  $\kappa = 40.6 k_B T$  and  $\gamma = 44.4$ , which agree with the values calculated from MD.

In the derivation of the elastic model, we only considered radial deformations in the forces equation as an approximation to the full 3D forces equations [11]. We expect that the major component of the surface deformation will be radial, but to check this assumption we performed an additional analysis on the ENM trajectory. The 2D-surfaces are constructed by binning atoms in  $\theta - \phi$  space and computing the average radial position within an element. Likewise, we can compute the average  $\theta$  and  $\phi$  positions within an element and the total displacement ( $ds$ ) of the element from it's mean position,  $ds^2 = dr^2 + r^2 d\theta^2 + r^2 \sin^2 \theta d\phi^2$ . By averaging over all elements and over all frames of the trajectory, we can compute the average contribution the radial displacement makes to the total displacement  $\langle dr^2/ds^2 \rangle = 0.73$ , and find that the deformation is dominated by the radial component.

We were interested in understanding the relative internal flexibility of the subunit proteins compared to the flexibility of the subunit interface. To explore this question, we assume the spherical harmonic coefficients of the fully flexible capsid (*flex*) can be partitioned between the projections of the internal subunit motions (*sub*) and projections from the interface motions with rigid subunits (*rig*)

$$\langle |\hat{a}_l|^2 \rangle_{flex} = \langle |\hat{a}_l|^2 \rangle_{sub} + \langle |\hat{a}_l|^2 \rangle_{rig} . \quad (9)$$

The  $\langle |\hat{a}_l|^2 \rangle_{flex}$  are known from the ENM trajectories presented in Fig. 1C,  $\langle |\hat{a}_l|^2 \rangle_{rig}$  can be calculated by constructing an ENM trajectory in which the subunits are treated as rigid units. Presumably the elastic parameters are changing between the rigid subunit network and the flexible network and therefore the scaling used to go between MD and the flexible ENM is no longer valid. Instead we assume that the lowest order mode ( $l = 0$ ) is fully captured by the rigid subunit motions and use the scaling factor  $\langle |\hat{a}_{l=0}|^2 \rangle_{flex} / \langle |\hat{a}_{l=0}|^2 \rangle_{rig}$ , to weight the  $\langle |\hat{a}_l|^2 \rangle_{rig}$ 's. The renormalized rigid subunit spectrum can be fit via Eq. 7 and we obtain  $Y_{rig} = 42.1 k_B T/\text{nm}^2$  and

$\kappa_{rig} = 81.6 k_B T$ . The difference between the flexible and rigid subunit spectra (Eq. 9), gives the spectrum for a network with flexible subunits and fixed interfaces. When we fit this spectrum we obtain  $Y_{sub} = 112.6 k_B T/nm^2$  and  $\kappa_{sub} = 72.1 k_B T$ , the spectra and associated fits are presented in the supplementary material in Fig S1. From the computed moduli, we observe that the subunit is nearly 3 times more resistive to stretching deformations than the interface, while the bending moduli of the interface and subunit have comparable stiffness values. Hence, a majority of the overall flexibility is coming from the subunit-subunit interface, while the subunit itself is relatively rigid. This is consistent with the observed change in behavior of the spectrum below wavelengths on the order of the subunit dimensions. Control of the subunit-subunit interaction strength should be the dominant mechanism for controlling virus flexibility; this can be viewed as a design principle [25].

In this work, we have provided a theoretical framework for the determination of the elastic properties,  $Y$  and  $\kappa$ , from the surface thermal fluctuations. We used atomic level simulations to measure the surface fluctuation spectrum and then showed agreement with the theoretical model, for the smallest class of virus capsid ( $T=1$ ), affirming the applicability of continuum theory to viruses. In addition to providing quantitative estimates of capsid elastic parameters, this work provides a methodology for calculating these properties without conducting a whole-capsid simulation, establishing a method that can be extended to larger capsid systems.

This work has been supported by the National Institutes of Health to CLB (RR012255) and by the National Science Foundation to ERM(DBI-0905773).

---

\* brookscl@umich.edu

- [1] V. S. Reddy, P. Natarajan, B. Okerberg, K. Li, K. V. Damodaran, R. T. Morton, C. L. Brooks III, and J. E. Johnson, *J Virol* **75**, 11943 (2001).
- [2] J. Lidmar, L. Mirny, and D. R. Nelson, *Phys Rev E Stat Nonlin Soft Matter Phys* **68**, 016 (2003).
- [3] T. T. Nguyen, R. F. Bruinsma, and W. M. Gelbart, *Phys Rev E Stat Nonlin Soft Matter Phys* **72**, 051923 (2005).
- [4] J. F. Conway, R. L. Duda, N. Cheng, R. W. Hendrix, and A. C. Steven, *J Mol Biol* **253**, 86 (1995).
- [5] D. E. Smith, S. J. Tans, S. B. Smith, S. Grimes, D. L. Anderson, and C. Bustamante, *Nature* **413**, 021 (2001).
- [6] D. N. Fuller, D. M. Raymer, V. I. Kottadiel, V. B. Rao, and D. E. Smith, *Proc Natl Acad Sci U S A* **104**, 16868 (2007).
- [7] A. Evilevitch, M. Castelnovo, C. M. Knobler, and W. M.

- Gelbart, *Journal of Physical Chemistry B* **108**, 6838 (2004).
- [8] I. L. Ivanovska, P. J. de Pablo, B. Ibarra, G. Sgalari, F. C. MacKintosh, J. L. Carrascosa, C. F. Schmidt, and G. J. L. Wuite, *Proc Natl Acad Sci U S A* **101**, 015 (2004).
- [9] J. P. Michel, I. L. Ivanovska, M. M. Gibbons, W. S. Klug, C. M. Knobler, G. J. L. Wuite, and C. F. Schmidt, *Proc Natl Acad Sci U S A* **103**, 023 (2006).
- [10] N. Kol, M. Gladnikoff, D. Barlam, R. Z. Shneck, A. Rein, and I. Rouso, *Biophys J* **91**, 767 (2006).
- [11] M. Widom, J. Lidmar, and D. R. Nelson, *Phys Rev E Stat Nonlin Soft Matter Phys* **76**, 031911 (2007).
- [12] Z. Yang, I. Bahar, and M. Widom, *Biophys J* **96**, 4438 (2009).
- [13] V. Sangita, P. S. Satheskumar, H. S. Savithri, and M. R. N. Murthy, *Acta Crystallogr D Biol Crystallogr* **61**, 1406 (2005).
- [14] E. Lindahl and O. Edholm, *Biophys J* **79**, 426 (2000).
- [15] E. R. May, A. Narang, and D. I. Kopelevich, *Phys Rev E Stat Nonlin Soft Matter Phys* **76**, 021913 (2007).
- [16] W. S. Klug, R. F. Bruinsma, J.-P. Michel, C. M. Knobler, I. L. Ivanovska, C. F. Schmidt, and G. J. L. Wuite, *Phys Rev Lett* **97**, 228101 (2006).
- [17] T. Gurin and R. Bruinsma, *Phys Rev E Stat Nonlin Soft Matter Phys* **76**, 061911 (2007).
- [18] L. Landau and E. Lifshitz, *Theory of Elasticity* (Pergamon Press, 1959).
- [19] M. Zink and H. Grubmüller, *Biophys J* **96**, 1350 (2009).
- [20] D. A. Case, *Current Opinion In Structural Biology* **4**, 285 (1994).
- [21] F. Tama and C. L. Brooks III, *J Mol Biol* **345**, 011 (2005).
- [22] P. Durand, G. Trinquier, and Y. H. Sanejouand, *Biopolymers* **34**, 759 (1994).
- [23] F. Tama, F. X. Gadea, O. Marques, and Y. H. Sanejouand, *Proteins* **41**, 1 (2000).
- [24] T. Cagin, M. Holder, and B. Pettitt, *J Comput Chem* **12**, 627 (1991).
- [25] R. V. Mannige and C. L. Brooks III, *PLoS One* **5**, e9423 (2010).

## FIGURES

FIG. 1. Structure and fluctuation spectrums of the SeMV mutant  $T=1$  capsid. (A) Outside and inside view of the capsid. Images were generated by VIPERdb from PDB:1x36. (B) Spectral intensities of surface fluctuations of SeMV trajectories from MD. Note mode  $l = 1$  for the icosahedrally constrained data set is  $\sim 10^{-28} nm^2$ , and is not shown. (C) Comparison of MD and ENM spectral intensities of surface fluctuations. The lines are fits from to the elastic model in Eq. 7, the solid line is the fit to the ENM data and the dashed line is the fit to the all-atom MD data.

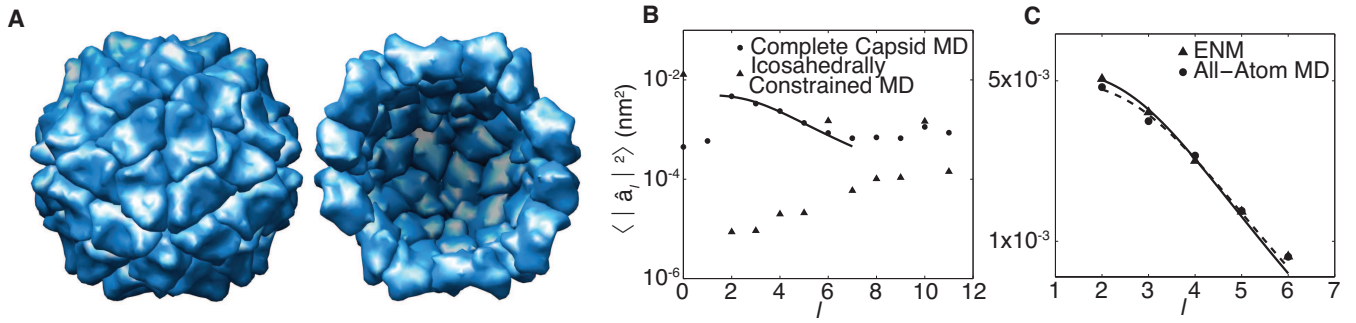


Figure 1

LW12074

23Mar2011